引用格式：XIN Lu, XIAO Wen, LIU Yakun, et al. Quantitative Monitoring of Morphological Change of Cancer Cells Apoptosis by Digital Holographic Microscopy (Invited)[J]. Acta Photonica Sinica, 2022, 51(10):1017001
辛露,肖文,刘雅坤,等.数字全息成像定量监测癌细胞凋亡过程形态变化(特邀)[J].光子学报,2022,51(10):1017001

数字全息成像定量监测癌细胞凋亡过程形态变化（特邀）

辛露[1],肖文[1],刘雅坤[1],张焕芝[2],李小平[2],潘锋[1]
(1 北京航空航天大学 仪器科学与光电工程学院,北京 100191)
(2 北京大学人民医院 妇产科,北京 100044)

摘　要:化疗药物敏感性测试中药物诱导的癌细胞凋亡的检测,对于实现更有效的个性化治疗具有重要意义。数字全息显微成像为癌细胞凋亡过程的检测提供了一种非侵入性的活细胞定量相位成像方法,能够满足细胞无标记、长时间成像以及药物作用下的细胞形态和动力学参数的评估。采用数字全息技术在无标记条件下对癌细胞加入药物后细胞凋亡过程进行动态连续成像记录,并对癌细胞相位图像进行数值再现,提取了细胞相位均值及细胞干重参数对癌细胞凋亡过程定量表征。实现结果表明,在癌细胞凋亡过程中,细胞相位值有不断增大的趋势,细胞面积减小,但细胞干重基本保持不变。而在细胞死亡破裂时,细胞相位值与细胞干重急剧减小,这可能是由于细胞膜破裂,细胞内物质流出导致的。这一结果也表明,数字全息显微成像能够为体外化疗药物敏感性检测提供了一种新的思路。

关键词:细胞凋亡;形态变化;数字全息成像;相位再现;细胞干重
中图分类号:TP29　　**文献标识码**:A　　**doi**:10.3788/gzxb20225110.1017001

0　引言

程序性细胞死亡(Programmed Cell Death,PCD)可由不同分子途径的激活引起[1],不同的细胞死亡过程具有不同的形态和生化特征。细胞凋亡是一种基因调控的程序性细胞死亡,通过消除生理冗余、物理损伤和异常细胞来控制多细胞生物和组织的发育[2]。放疗和化疗对于癌症患者术前和术后的治疗是必不可少的。化疗药物主要通过促进癌细胞凋亡来破坏癌细胞并抑制其增殖。抗癌药物的功效是通过它们识别癌细胞和选择性地促进其凋亡的能力来衡量的。抗癌药物敏感性测试(Drug Sensitivity Test, DST)是一种根据敏感性确定治疗肿瘤最有效药物的方法。肿瘤的基因型和发病机制各不相同,肿瘤可能对一种或多种药物产生耐药性,或对多种药物表现出敏感性[3]。因此,检测DST中药物诱导的癌细胞凋亡,对于降低耐药性和提高药敏试验的效率,实现更有效的个性化治疗具有重要意义[4]。目前检测细胞凋亡的方法主要通过检测与细胞凋亡相关的细胞形态和表面标志物的变化。

在整个有机体中,细胞凋亡会导致细胞的受控分解,从而避免任何细胞内介质的释放,但在体外,细胞凋亡会进入继发性坏死的终末期,导致细胞膜完整性的丧失以及随后细胞内容物释放到周围细胞外空间[5-6]。流式细胞术、膜蛋白[7]、TUNEL分析[8]等方法对细胞凋亡判别的特异性较差。而细胞凋亡过程会表现出典型的、明确的形态学变化,包括质膜起泡、染色质浓缩以及核断裂和凋亡小体的形成等[9-10]形态学标准被认为是细胞凋亡的最可靠依据[11]。

数字全息显微(Digital Holographic Microscopy,DHM)是一种干涉成像技术,可以无创地提供与细胞固有特性相关的丰富的细胞内信息。它可以根据折射率(Refractive Index,RI)对比度识别无标记细胞,而无需

基金项目:北京市自然科学基金(No. M22017)
第一作者:辛露(1993—),女,博士研究生,主要研究方向为数字全息显微成像及其生物医学应用。Email: xinlu18@buaa.edu.cn
导师(通讯作者):潘锋(1979—),男,副教授,博士,主要研究方向为数字全息术及工程与医学应用。Email: panfeng@buaa.edu.cn
收稿日期:2022-06-30;**录用日期**:2022-09-16

对细胞进行荧光标记[12]，因此在生物医学领域有着广泛的应用，如细胞计数[13]、疾病诊断[14-15]、癌细胞分离[16-17]、治疗评估[18]。细胞的RI是一个固有的光学参数，它描述了光穿过细胞产生的光程差，与细胞的生物物理特性相关。此外，DHM能够提供定量地相位信息，这使得它与大多数仅能收集光强度的传感器有很大不同。而定量相位图像除了能够提供有关形态学的信息外，还能够计算整个细胞内的干重(Dry Mass，DM)[19-21]。因此数字全息显微成像技术被用来对细胞生长过程及生理活动进行动态监测，如细胞分裂[22]、细胞迁移[23]、细胞在外界刺激下的形态变化[24-27]等。

本文采用数字全息显微成像方法对化疗药物诱导的癌细胞凋亡过程中的形态变化进行记录与分析。实验过程中，通过对卵巢癌细胞A2780加入临床治疗中常用的化疗药物顺铂诱导癌细胞凋亡，利用数值方法再现出癌细胞完整的凋亡过程及细胞膜破裂的定量相位图像，进而从中提取细胞形态参数相位均值及细胞干重对癌细胞凋亡过程中的形态变化进行表征。结果表明，生长状态的癌细胞与凋亡期及死亡细胞的相位图像及其形态参数上有极为明显的差异。因此，本文方法能够在无需荧光标记的情况下对癌细胞的凋亡细胞和死细胞进行区分，为个体化治疗中的体外药敏试验确定和选择最有效的化疗药物，并确定其有效剂量提供一种更加经济、方便的检测方法。

1 材料及方法

1.1 细胞培养

本文研究的细胞系为上皮性卵巢癌细胞A2780细胞。细胞培养过程中，A2780细胞生长在1640(RPMI Medium 1640 basic 1X，GIBCO，中国)培养基中，培养基中添加l-谷氨酰胺、15 mmol/L HEPES和10% 胎牛血清(GIBCO 10099-141，澳大利亚)。培养环境为5% CO_2，温度为37℃。将癌细胞接种于35 mm的Willco玻璃培养皿中，培养24 h后，将化疗药物顺铂(Sigma-Aldrich，Steinheim，德国)加入培养基中，最终培养基中顺铂药物浓度为20 μg/mL。加入药物之后，立即将细胞培养皿置于观测平台上进行细胞成像。

1.2 数字全息显微图像记录

采用离轴式数字全息显微成像系统对细胞进行成像[28]，光路结构及光路示意如图1，该系统单次相机曝光即可实现复杂的物体波前重建。系统光源选用相干激光器(532 nm，100 mW)，通过单模光纤输出。光束从激光器发出后，由准直透镜(L)产生平面光波，然后激光束经由偏振分光棱镜(Polarization Beam Splitter，PBS)分为两路，即物光路和参考光路。PBS前面的半波片(Half Wave Plate，HWP1)用于调整两个光束之间的强度比。参考光路中的另一个半波片(HPW2)，使参考光波的偏振方向与物光波一致。物光波经由反射镜M2反射后，通过会聚透镜(Converge Lens，CL)后透射穿过待测样品，然后，由显微物镜(Microscopic Objective，MO)和套筒透镜(Tube Lens，TL)构成的显微成像部件对待测样品放大成像，并通过分光棱镜(Beam Splitter，BS)与参考光波在CCD相机成像面发生干涉，产生细胞干涉图，并由CCD相机记录。发生

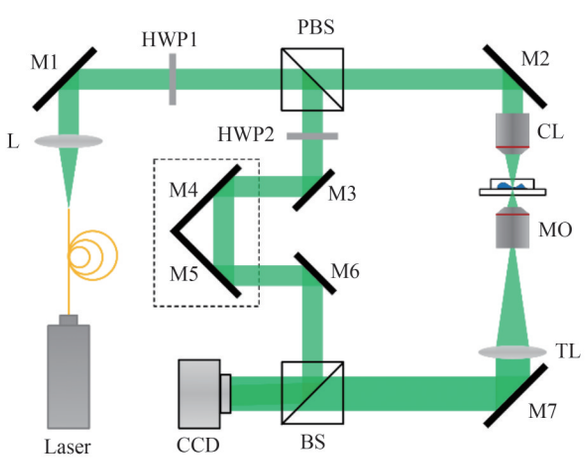

图1 离轴数字全息显微成像系统光路结构示意

Fig. 1 Optical path structure of off-axis digital holographic microscopic imaging system

干涉时，在显微镜MO固定的情况下，调节待测物体的高度使其位于MO的焦点，由于CL与MO组成共焦系统，因此调节CL的位置使待测细胞同样位于其焦面位置，然后调节透镜TL使其出射光为平面波。同时，参考光路中的反射镜M4、M5用于在多个方向上调节参考光与物光之间的夹角，使记录的全息图像的零级像、+1级像和-1级像相互分离，实现离轴全息成像。显微物镜MO选用奥林巴斯20倍平场半复消色差物镜（Olympus UPLFLN 20），其数值孔径为NA=0.50。记录全息图像采用的相机为加拿大由PointGrey公司生产的由FlyCapture软件控制的相机，像素数为2 048×2 048，其单个像素尺寸为5.5 μm，因此成像系统的分辨率约为0.275 μm。在细胞成像过程中，细胞贴壁生长于细胞培养皿底部，培养皿中填满细胞培养液保证细胞正常生长。从细胞培养液中加入药物开始，相机每1 min记录一张全息图像，共记录9 h。

1.3 细胞形态参数计算

1.3.1 细胞相位图像再现处理过程

全息干涉图像由物光波和参考光波叠加形成，全息图的再现过程是利用原参考光$R(x,y)$照射全息图实现，在全息面得到的衍射光波包括了为零级衍射光、+1级衍射光和-1级衍射光。在离轴全息成像中，物光波和参考光波发生干涉时存在一定的夹角，再现得到的零级衍射项、+1级衍射项和-1级衍射项三部分也具备一定的夹角。由于离轴全息的三个衍射级次各自分离，因此单次曝光即可实现独立获取每个衍射项，更加适用于快速测量的需要。

对数字图像形式记录的细胞全息图像，经过数值衍射再现过程能够得到反映细胞折射率信息的相位图像。首先，在进行衍射再现之前，需要对全息图像进行切趾[29]和空间滤波[30]。切趾操作是将全息图像乘以一个二维三次样条插值函数，去除由于CCD的大小有限所产生的衍射条纹对波前的影响。由于离轴记录的全息图像的零级像、+1级像和-1级像相互分离，因此通过将全息图的空间频谱乘以一个带通空间滤波器对全息图像进行滤波即可得到单独的衍射项。然后，采用角谱传播算法对全息图像进行数值传播[31]，该方法的优势在于无论传播距离如何，目标图像的大小保持不变。为了消除由于显微物镜的使用、光学元件的缺陷以及实验系统等因素产生的像差对计算细胞相位的影响，采用基于泽尼克多项式模型的数值参数透镜（Numerical Parametric Lenses，NPL）的数值方法来补偿像差[32-33]。此外，数字全息具备进行数值重聚焦的能力，通过对细胞区域计算出最佳的传播距离[34]，来补偿图像记录过程中产生的细胞离焦。最后，对细胞相位图像进行解包裹，将约束在-π和π之间的相位值进行解构[35]，即可得到数值连续的细胞相位图像。

1.3.2 细胞相位及干重参数计算

为了计算单个细胞在死亡的过程中形态随时间的变化，采用最大类间方差阈值分割方法将单个细胞从背景相位中分割出来。由全息记录重建的细胞相位图像实际上是由于细胞与培养液之间的折射率不同，照明光波在经过不同区域时产生的相位差，即

$$\Delta\varphi(x,y)=\varphi_{\mathrm{m}}(x,y)-\varphi_{\mathrm{c}}(x,y)=\frac{2\pi}{\lambda}h(x,y)(n_{\mathrm{m}}(x,y)-n_{\mathrm{c}}) \tag{1}$$

式中，λ为照明光波的波长（532 nm），n_{c}为细胞周围培养液的折射率，n_{m}和h分别为细胞在位置(x,y)处的折射率及厚度。因此，取细胞区域的像素相位均值$\Delta\bar{\varphi}$来反映细胞整体的厚度和折射率信息。此外，细胞的相位图像能够用来计算细胞内干物质的质量，即细胞的干重，其计算方法为

$$D_{\mathrm{M}}=\frac{\lambda}{2\pi\alpha}\int_{S_{\mathrm{c}}}\Delta\varphi\mathrm{d}s=\frac{\lambda}{2\pi\alpha}\Delta\bar{\varphi}S_{\mathrm{c}} \tag{2}$$

式中，S_{c}为细胞区域的面积。α是一个与细胞内含量有关的常量，称为特定折射增量[17]，约为0.18～0.21 mL/g，通常取α为0.2 mL/g。因此，细胞内的干重与细胞相位均值和细胞区域的面积相关。

2 实验结果

2.1 癌细胞死亡过程相位图再现结果

实验过程中，将培养皿中贴壁生长的癌细胞在加入药物前置于数字全息显微观测平台上采集一张全息图像，并在加入药物后每1 min采集一张全息图像，实验过程进行9 h，共采集540张全息图。之后将采集到的全息图进行数值重建，得到相位图像，图2（a）和（b）分别为加入药物前及加入药物9 h后相位图像。从相

位图像能够很明显看出，大部分细胞已经破裂死亡，图中箭头所指向的是8个已经明显破裂死亡的细胞，而其他没有破裂的细胞也产生了明显的收缩，细胞相位值有明显增大。为了更加清晰地展示细胞的死亡过程，选取其中两个破裂的细胞，细胞2和细胞6，并在图3中展示了5 h死亡过程中细胞形态的相位图像。图3中能够较为直观地看出，细胞在破裂死亡前细胞面积减小，相位值变大，细胞在产生向内收缩的现像。当收缩达到一定程度，分别在4 h 35 min和4 h 9 min时，细胞2和细胞6细胞相位值不再增大而是突然减小，表明细胞发生破裂，细胞内物质流出失去活性，此后细胞相位值不再发生明显的变化。

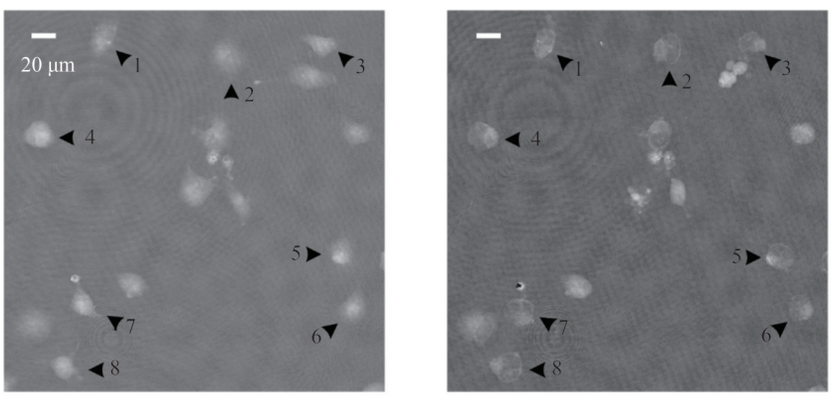

(a) Phase image of A2780 cells before drug　(b) Phase image of A2780 cells with drug for 9 h

Fig. 2　A2780细胞加药前与加药9 h后的相位图像

Fig. 2　Phase images of A2780 cells before drug and with drug for 9 h

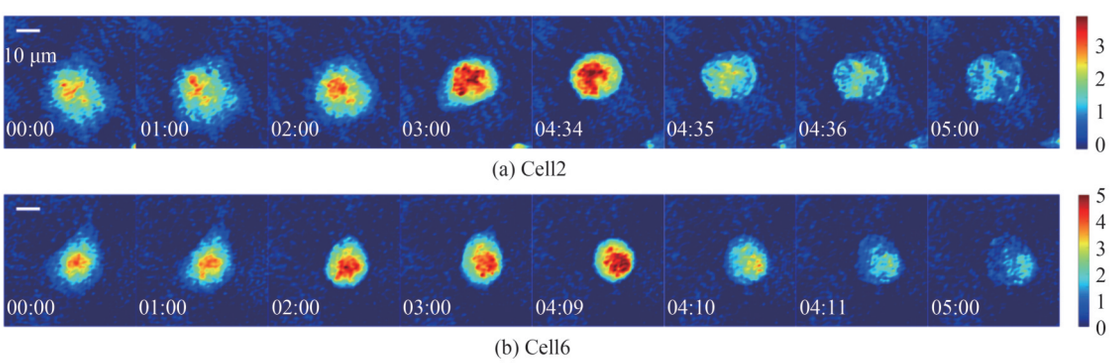

Fig.3　加药后癌细胞调亡过程中形态随时间变化

Fig. 3　Morphological changes of cancer cells death after exposing to drug

2.2　癌细胞凋亡过程参数变化

为了更加准确地描述癌细胞产生破裂死亡过程中的形态变化，对图2中的8个细胞的形态参数进行了计算。图4中的8条曲线分别展示了细胞的平均相位的变化，每条曲线由90个时间点组成，每小时取10个时间点，即每个点由6个时刻的细胞相位均值再取平均得到。如图4所示，图中的曲线为细胞相位的平均值，阴影部分为标准差。从图中的曲线可以看出，在加药后细胞的平均相位值均呈现出增大的趋势，直至在某一个时刻相位值突然减小，这一过程与图3中观察到的细胞相位图像变化相一致。细胞在内外渗透压平衡的活性状态下，体积不会出现较大的变化，结合图3中细胞面积减小的变化过程，表明细胞在收缩过程中引细胞高度或内部折射率在不断增加。但不同细胞相位均值的变化过程存在差异，不同于其他细胞的逐渐增大的过程，细胞5和细胞6均出现相位均值大幅回落后又重新升高的现象。然而，细胞在破裂前的整体趋势均为细胞相位值的增加。

对细胞内干重的计算结果如图5。从图中的8条曲线可以看出，细胞破裂前，在对应的细胞相位均值明显增大且趋势不一的情况下，细胞的干重均没有发生明显的变化，只在细胞破裂时干重瞬间减小。细胞干重代表了细胞内干物质的质量，因此这一趋势可能是由于细胞破裂时，细胞内部物质流出导致的干重急剧

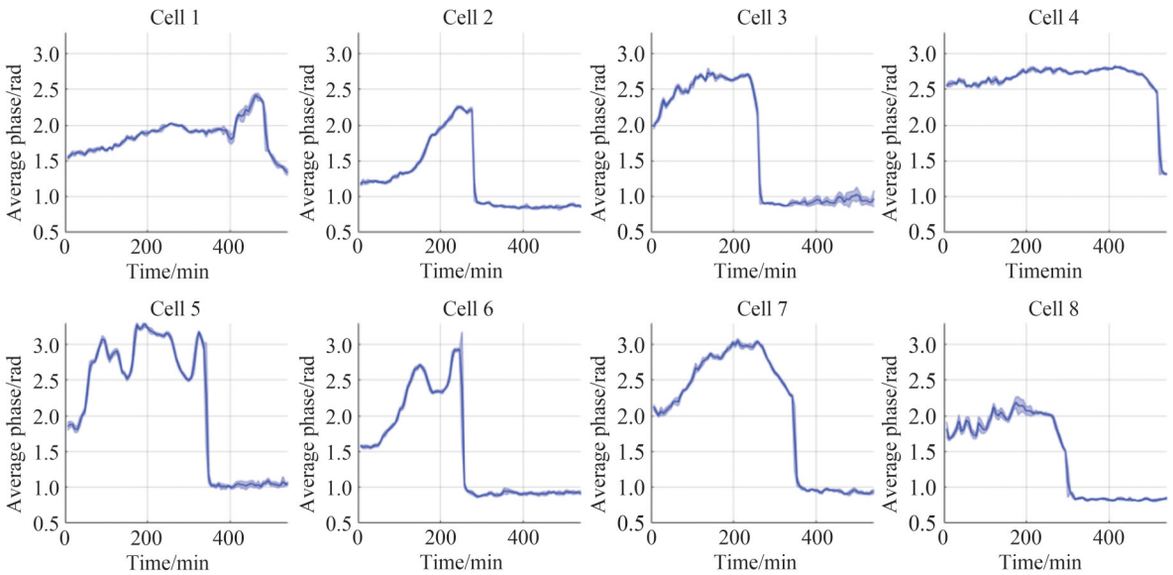

Fig. 4　癌细胞调亡过程中相位均值随时间的变化

Fig. 4　Changes of mean phase shift with time in the process of cancer cell death

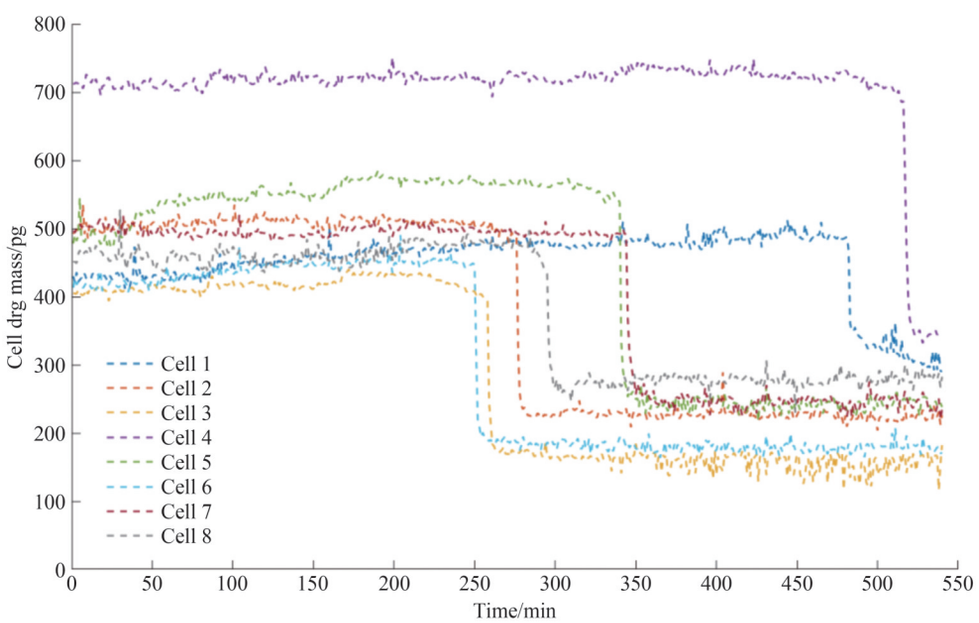

Fig. 5　癌细胞调亡过程中细胞干重随时间的变化

Fig. 5　Changes of cell dry mass with time in the process of cancer cell death

较少。从图5中能够看出，细胞4的干重相比其他细胞都较大，这是由于同种细胞不同个体之间存在一定的差异，且癌细胞具有较强的异质性，因此不同细胞的形态是有差异的，但从图中也能看出，差异较大的细胞在破裂的过程所表现出的干重变化趋势是一致的。这一结果也表明由数字全息相位图像计算所得的细胞参数能够对癌细胞凋亡的变化过程进行表征。

3　结论

本文采用数字全息显微系统对无任何化学标记的癌细胞加入药物后的细胞形态变化过程进行了记录。通过对记录的全息干涉图像进行切趾、频域滤波、角谱传播、像差补偿及数值自动聚焦等过程完成了对细胞相位图像的数值再现。为了对癌细胞在化疗药物下凋亡过程中细胞形态变化进行分析，从相位图像中分割出单个细胞相位图像，提取其相位均值及细胞干重并绘制出其参数变化曲线。结果表明，癌细胞在凋亡至

裂解前，细胞干重没有较明显的变化，而在细胞膜裂解瞬间，细胞内物质流出，细胞干重急剧减小。而细胞相位均值在裂解前不断增大，而细胞干重并未明显增大表明细胞出现了收缩，这与已有研究中的细胞形态变化的结论一致。因此，数字全息显微技术提供的定量相位图像能够反映癌细胞凋亡的特异性形态变化，能够在无需荧光标记的情况下对癌细胞的凋亡细胞和死细胞进行区分，对体外抗癌药物的筛选及个性化治疗具有重要意义。

参考文献

[1] KRYSKO D V, BERGHE T V, D'HERDE K, et al. Apoptosis and necrosis: detection, discrimination and phagocytosis[J]. Methods, 2008, 44(3): 205-221.

[2] TARAPHDAR A K, ROY M, BTTACHARYA R K. Natural products as inducers of apoptosis: implication for cancer therapy and prevention[J]. Current Science, 2001: 1387-1396.

[3] BALYAN J, KRIZOVA A, GUNULEC J, et al. Multimodal holographic microscopy: distinction between apoptosis and oncosis[J]. PloS one, 2015, 10(3): e0121674.

[4] LIU Kuan, LIU Pengcheng, LIU Run, et al. Dual AO/EB staining to detect apoptosis in osteosarcoma cells compared with flow cytometry[J]. Medical Science Monitor Basic Research, 2015, 21: 15.

[5] WOLDERS F, ANDERSSON H, VAN DEN BERG A, et al. Apoptosis induced kinetic changes in autofluorescence of cultured HL60 cells-possible application for single cell analysis on chip[J]. Apoptosis, 2004, 9(6): 749-755.

[6] DUPREZ L, WIRAWAN E, BERGHE T V, et al. Major cell death pathways at a glance[J]. Microbes and Infection, 2009, 11(13): 1050-1062.

[7] KRYSKO, DE RIDDER L, CORNELISSEN M. Phosphatidylserine exposure during early primary necrosis (oncosis) in JB6 cells as evidenced by immunogold labeling technique[J]. Apoptosis, 2004, 9(4): 495-500.

[8] FREUDE B, MASTERS T N, KOSTIN S, et al. Cardiomyocyte apoptosis in acute and chronic conditions[J]. Basic Research in Cardiology, 1998, 93(2): 85-89.

[9] SHI Yigong. Mechanisms of caspase activation and inhibition during apoptosis[J]. Molecular Cell, 2002, 9(3): 459-470.

[10] MOUJALLED D, STRASSER A, LIDDERL J R. Molecular mechanisms of cell death in neurological diseases[J]. Cell Death & Differentiation, 2021, 28(7): 2029-2044.

[11] MAHDI E J, ALSHAHRANI A M, ABDULSATAR A A, et al. Morphological evaluation of apoptosis induced by salicylates in HT-1080 human fibrosarcoma cells[J]. Journal of Microscopy and Ultrastructure, 2014, 2(1): 20-27.

[12] SEO S, SU T W, TSENG D K, et al. Lensfree holographic imaging for on-chip cytometry and diagnostics[J]. Lab on a Chip, 2009, 9(6): 777-787.

[13] RA H K, KIM H, YOON H J, et al. A robust cell counting approach based on a normalized 2D cross-correlation scheme for in-line holographic images[J]. Lab on a Chip, 2013, 13(17): 3398-3409.

[14] UGELE M, WENIGER M, LEIDENDERGER M, et al. Label-free, high-throughput detection of P. falciparum infection in sphered erythrocytes with digital holographic microscopy[J]. Lab on a Chip, 2018, 18(12): 1704-1712.

[15] LENZ P, BETTENWORTH D, KRAUSEWITZ P, et al. Digital holographic microscopy quantifies the degree of inflammation in experimental colitis[J]. Integrative Biology, 2013, 5(3): 624-630.

[16] ROITSHTAIN D, WOLBROMSKY L, BAL E, et al. Quantitative phase microscopy spatial signatures of cancer cells[J]. Cytometry Part A, 2017, 91(5): 482-493.

[17] RUBIN M, STEIN O, TURKO N A, et al. TOP-GAN: Stain-free cancer cell classification using deep learning with a small training set[J]. Medical Image Analysis, 2019, 57: 176-185.

[18] BELASHOV V, ZHIKHOREVA A A, BELYAEVA T N, et al. Digital holographic microscopy in label-free analysis of cultured cells′ response to photodynamic treatment[J]. Optics Letters, 2016, 41(21): 5035-5038.

[19] BARER R, TKACZYK S. Refractive index of concentrated protein solutions[J]. Nature, 1954, 173(4409): 821-822.

[20] POPESCU G, PARK Y K, LUE N, et al. Optical imaging of cell mass and growth dynamics[J]. American Journal of Physiology-Cell Physiology, 2008, 295(2): C538-C544.

[21] GHENIM L, ALLIER C, OBEID P, et al. A new ultradian rhythm in mammalian cell dry mass observed by holography[J]. Scientific Reports, 2021, 11(1): 1-11.

[22] ZLOTEK-ZLOTKIEWICZ E, MONNIER S, CAPPELLO G, et al. Optical volume and mass measurements show that mammalian cells swell during mitosis[J]. Journal of Cell Biology, 2015, 211(4): 765-774.

[23] JANICKE B, KARSNAS A, EGELBERG P, et al. Label-free high temporal resolution assessment of cell proliferation using digital holographic microscopy[J]. Cytometry Part A, 2017, 91(5): 460-469.

[24] LEE Y H, LEE C C, HUANG C H, et al. Laminar shear stress promotes nicotine-induced inflammation and hemostatic expression in human endothelial cells[J]. Cellular and Molecular Bioengineering, 2016, 9(3): 466-477.

[25] FEUTH M, VICAR T, GUMULEC J, et al. Quantitative phase dynamics of cancer cell populations affected by blue light[J]. Applied Sciences, 2020, 10(7): 2597.

[26] CAO Runyu, XIAO Wen, WU Xintong, et al. Quantitative observations on cytoskeleton changes of osteocytes at different cell parts using digital holographic microscopy[J]. Biomedical Optics Express, 2018, 9(1): 72-85.
[27] CAO Runyu, XIAO Wen, PAN Feng, et al. Displacement and strain mapping for osteocytes under fluid shear stress using digital holographic microscopy and digital image correlation[J]. Biomedical Optics Express, 2021, 12(4): 1922-1933.
[28] MARQUET P, RAPPAZ B, MAGISTRETTI P J, et al. Digital holographic microscopy: a noninvasive contrast imaging technique allowing quantitative visualization of living cells with subwavelength axial accuracy[J]. Optics Letters, 2005, 30(5): 468-470.
[29] CUCHE E, MARQUET P, DEPEURSINGE C. Aperture apodization using cubic spline interpolation: application in digital holographic microscopy[J]. Optics Communications, 2000, 182(1-3): 59-69.
[30] CUCHE E, MARQUET P, DEPEURSINGE C. Spatial filtering for zero-order and twin-image elimination in digital off-axis holography[J]. Applied Optics, 2000, 39(23): 4070-4075.
[31] DE NICHLA S, FINIZIO A, PIERATTINI G, et al. Angular spectrum method with correction of anamorphism for numerical reconstruction of digital holograms on tilted planes[J]. Optics Express, 2005, 13(24): 9935-9940.
[32] COLOMB T, MONTFORT F, KUHN J, et al. Numerical parametric lens for shifting, magnification, and complete aberration compensation in digital holographic microscopy[J]. Journal of the Optical Society of American A, 2006, 23(12): 3177-3190.
[33] XIAO Wen, XIN Lu, CAO Runyu, et al. Sensing morphogenesis of bone cells under microfluidic shear stress by holographic microscopy and automatic aberration compensation with deep learning[J]. Lab on a Chip, 2021, 21(7): 1385-1394.
[34] MEMMOLO P, DISTANTE C, PATURZO M, et al. Automatic focusing in digital holography and its application to stretched holograms[J]. Optics Letters, 2011, 36(10): 1945-1947.
[35] GHIGLIA D C, ROMERO L A. Robust two-dimensional weighted and unweighted phase unwrapping that uses fast transforms and iterative methods[J]. Journal of the Optical Society of America A, 1994, 11(1): 107-117.

Quantitative Monitoring of Morphological Change of Cancer Cells Apoptosis by Digital Holographic Microscopy (Invited)

XIN Lu[1], XIAO Wen[1], LIU Yakun[1], ZHANG Huanzhi[2], LI Xiaoping[2], PAN Feng[1]
(1 *Key Laboratory of Precision Opto-mechatronics Technology, School of Instrumentation & Optoelectronic Engineering, Beihang University, Beijing* 100191, *China*)
(2 *Department of Obstetrics and Gynecology, Peking University People's Hospital, Beijing* 100044, *China*)

Abstract: Radiotherapy and chemotherapy are essential for preoperative and postoperative treatment of cancer patients. Chemotherapy drugs destroy cancer cells and inhibit their proliferation mainly by promoting cancer cell apoptosis. The efficacy of anticancer drugs is measured by their ability to recognize cancer cells and selectively promote their apoptosis. The Drug Sensitivity Test (DST) is a method to determine the most effective drug for tumor treatment according to the sensitivity. Tumors may be resistant to one or more drugs, or show sensitivity to multiple drugs for their different genotype and pathogenesis. Therefore, the detection of drug-induced apoptosis in anticancer drug sensitivity test is of great significance for reducing drug resistance, improving the efficiency of drug sensitivity test and achieving more effective personalized treatment. At present, the main methods to detect apoptosis are to detect the changes of cell morphology and surface markers related to apoptosis. However, the commonly used methods like flow cytometry, membrane protein, TUNEL analysis, have poor specificity in the detection of cell apoptosis. The typical morphological changes exhibited in the process of apoptosis which have become a reliable basis for the identification of apoptosis. Digital holographic microscopy provides a non-invasive quantitative phase imaging method for living cells. It can meet the requirements of label-free, long-term imaging, and evaluation of cell morphological and kinetic parameters under different treatments. In this paper, digital holographic microscopy is used to record images of label-free cancer cells during apoptosis process after adding drugs. Firstly, a Mach-Zehnder digital holographic microscopic system with an off-axis configuration is used to capture the wave-field of cancer cells. This system can realize complex object wavefront reconstruction with a single camera exposure. In the process of cell imaging, the cells adhere to

the bottom of the cell culture dish, and the culture dish is filled with cell culture solution to ensure the normal growth of cells. The camera records a hologram every 1min for a total of 9 hours after adding drugs into the cell culture solution. Then, the phase images of cancer cells are numerically reconstructed. Two pre-processing operations are implemented, consisting of hologram apodization and spatial filtering and then the angle spectrum reconstruction algorithm is employed to implement the numerical propagation, keeping the object image size constant whatever the propagation distance. To obtain an in-focus and sharp object image, an optimal propagation distance needs to be found by automatic focus method. Besides, Numerical Parametric Lenses (NPL) method is employed to compensate the phase aberrations in the phase image. Due to the phase value reconstructed from the hologram constrained between $-\pi$ and π, the continuous phase map of the object can be retrieved by phase unwrapping. From the reconstructed phase image of cells after 9 hours of drug treatment, it can be clearly seen that most of the cells have broken and died, while other cells that have not broken have also shrunk significantly, and the cell height has increased significantly. Furthermore, we select 8 cells from the dead cells for further analysis of their complete death process. Single-cell phase images are segmented from the phase images. And, the morphological change of cell apoptosis process is characterized morphologically by the average phase shift and dry mass. It can be seen from the change carves of these two parameters during the cell apoptosis, there is no obvious change of cell dry mass before apoptosis. But at the moment of the cells lose membrane integrity and release their intracellular contents, cells′ dry mass decreased sharply. At the meantime, the average phase shift continuously increases before the cells lose membrane integrity, indicating that the cells have contracted, which is consistent with the conclusion in previous study. These results show that there are significant differences in phase images and morphological parameters between growing cancer cells and apoptotic and dead cells. Therefore, the method in this paper can distinguish apoptotic cells and dead cells without fluorescent labeling. And it can provide a more economical and convenient detection method for determining and selecting the most effective chemotherapeutic drugs and determining their effective dose for in vitro drug sensitivity test in individualized treatment.

Key words: Cancer cell apoptosis; Morphological change; Digital holography; Phase reconstruction; Cell dry mass

OCIS Codes: 170.1530; 090.1995; 030.1670

Foundation item: Natural Science Foundation of Beijing (No. M22017)